


Article

Microstructure and Mechanical Properties of Diamond–Ceramic Composites Fabricated via Reactive Spark Plasma Sintering

Yunwei Shi ¹, Lanxin Hu ², Aiyang Wang ¹, Chun Liu ³, Qianglong He ^{1,*}  and Weimin Wang ¹

¹ School of Materials Science and Engineering, Wuhan University of Technology, Wuhan 430070, China; 1917069803@whut.edu.cn (Y.S.); aywang@whut.edu.cn (A.W.); shswmwang@whut.edu.cn (W.W.)

² School of Mechanical Engineering, Wuhan Business University, Wuhan 430056, China; nancyhu2023@163.com

³ School of Mechanical Engineering, Hunan Institute of Science and Technology, Yueyang 414006, China; chunliu@hnist.edu.cn

* Correspondence: shsqlhe@whut.edu.cn

Abstract: In order to prepare diamond composites with excellent mechanical properties under non-extreme conditions, in this study, a diamond–ceramic composite was successfully prepared via reactive spark plasma sintering using a diamond–Ti–Si powder mixture as the raw material. The microstructures and mechanical properties of the diamond–ceramic composite sintered at different temperatures were studied. When the sintering temperature was 1500 °C, the diamond–ceramic composite exhibited a volume density of 3.65 g/cm³, whereas the bending strength and fracture toughness were high at 366 MPa and 6.17 MPa·m^{1/2}, respectively. In addition, variable-temperature sintering activated the chemical reaction at a higher temperature, whereas lowering the temperature prevented excessive graphitisation, which is conducive to optimising the microstructure and mechanical properties of the composite.

Keywords: diamond–ceramic composite; sintering temperature; microstructure; mechanical properties



Citation: Shi, Y.; Hu, L.; Wang, A.; Liu, C.; He, Q.; Wang, W. Microstructure and Mechanical Properties of Diamond–Ceramic Composites Fabricated via Reactive Spark Plasma Sintering. *Ceramics* **2024**, *7*, 1390–1400. <https://doi.org/10.3390/ceramics7040090>

Academic Editors: Malika Saadaoui and Gilbert Fantozzi

Received: 28 August 2024

Revised: 27 September 2024

Accepted: 1 October 2024

Published: 2 October 2024



Copyright: © 2024 by the authors. Licensee MDPI, Basel, Switzerland. This article is an open access article distributed under the terms and conditions of the Creative Commons Attribution (CC BY) license (<https://creativecommons.org/licenses/by/4.0/>).

1. Introduction

Diamond is an allotrope of graphite, and natural diamond is an elemental crystal formed from carbon under high pressure and temperature deep in the earth. Because the C–C bonds in diamond are extremely strong, all the valence electrons form covalent bonds, leaving no free electrons. Therefore, diamond has an extremely high hardness, making it the hardest substance in nature, with a Mohs hardness of grade 10 and microhardness of 10,000 kg/mm² [1,2]. These excellent mechanical properties provide a diamond with outstanding tribological properties and better wear resistance than those of cemented carbides and ceramics. Moreover, using diamond as a processing tool not only improves processing efficiency but also increases precision surface [3]. The application of diamond tools solves the processing problems of various difficult-to-process materials, thereby guaranteeing the application and promotion of new tools and materials [4].

The carbon atoms in the diamond lattice structure are bonded via strong covalent bonds, with no impurities or defects present. Owing to the high sound speed and elastic modulus, heat transfers quickly through the diamond, resulting in high thermal conductivity of approximately 2000 W/m·K at room temperature, which is five times that of Cu (400 W/m·K). Therefore, in addition to its use in processing tools, diamond is often combined with metals for thermal management in electronic components [5,6].

In these applications, diamonds are often prepared as diamond–metal composites [7–9]. However, these composites deteriorate rapidly at high temperatures. To address this issue, diamond–ceramic composites are being developed [10–13]. Typically, the preparation of diamond–ceramic composite requires extreme conditions [14]. For example, Jaworska et al. fabricated diamond–ceramic layers in diamond-stable conditions at a high pressure and temperature of 8 GPa and 1800 °C [15], respectively. Lai et al. prepared B₄C–diamond

ceramics with high toughness via high-pressure sintering at 5 GPa and 1600 °C [16]. Previous studies have shown that under oxygen-free conditions, diamonds tend to graphitise at 750 °C [17]. However, the extremely high pressures involved in these studies inhibited the graphitisation of diamond, which would have caused the rapid deterioration of its properties. Additionally, because of the rapid heating rate of spark plasma sintering, diamond graphitisation was suppressed to a certain extent [18]. To further weaken the influence of diamond graphitisation on the properties of the composites, carbide-forming elements such as Si, Ti, and B are added to the diamond. These elements react with C to form SiC, TiC, and B₄C, which possess high hardness and are chemically bonded to diamond, thus effectively holding the diamond particles [19,20].

As shown in Figure 1, the Gibbs free energy of the reaction of Ti with C is significantly more negative than that of B or Si with C, indicating that Ti reacts more readily with C than B or Si. Therefore, Ti can play the role of consuming graphite. Although the reaction between B and C is as difficult as that between Si and C, Si has a high melting point of 1410 °C, and its liquid phase sintering significantly promotes densification [21]. Taking the above factors into consideration, in order to achieve the preparation of diamond composites with excellent mechanical properties under non-extreme conditions, Ti and Si were selected as absorbents to adsorb the products of diamond graphitisation and combined with spark plasma sintering to fabricate diamond–ceramic composites.

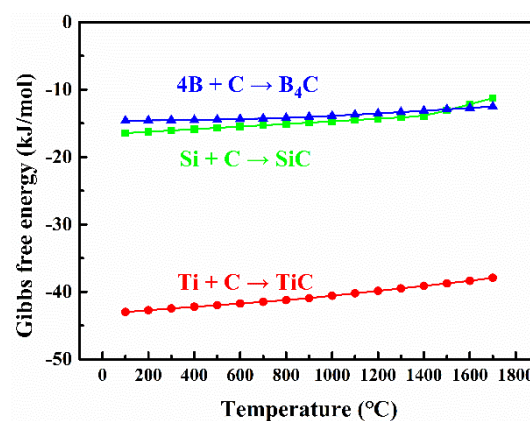


Figure 1. Gibbs free energy of the reaction of B/Si/Ti with C.

2. Experimental Procedure

Commercially available diamond (purity = 99%, 800 mesh, Fandeng Industry and Trade Co., Ltd., Yongkang, China), Ti (purity = 99.99%, ≥300 mesh, Shanghai Aladdin Biochemical Technology Co., Ltd., Shanghai, China), and Si powders (purity = 99.9%, 1–3 µm, Shanghai Aladdin Biochemical Technology Co., Ltd., Shanghai, China) were used as raw materials.

Figure 2 shows the SEM images and corresponding XRD patterns of the diamond, Ti, and Si powders. As shown in Figure 2A,C, the powder particle sizes of diamond and Ti are larger than those of Si. The average size of the diamond particles was approximately 20 µm, and the size distribution was uniform. Ti powder exhibited a larger average particle size; however, its size distribution was not uniform. The large Ti particles were 50 µm, whereas the smaller Ti particles were <10 µm. Furthermore, as shown in Figure 2E, the size of the Si particles was small. In addition, no impurity peaks were observed in the XRD patterns of the diamond, Ti, and Si powders (Figure 2B,D,F), confirming their high purity.

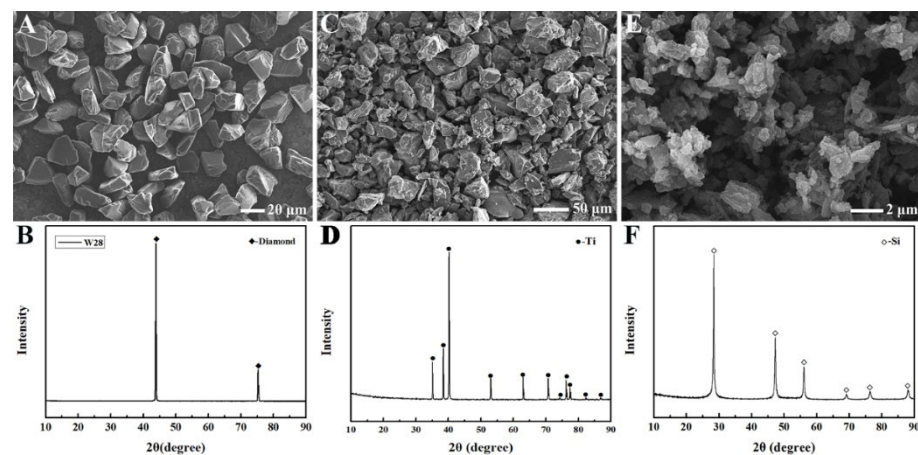


Figure 2. SEM images and corresponding XRD patterns of the raw materials: (A,B) diamond; (C,D) Ti; and (E,F) Si.

The diamond, Ti, and Si powders were weighed in a 4:3:3 mass ratio and placed in a 250 mL polyethylene jar. After injecting anhydrous ethanol into the jar, the mixture was milled using a planet mill (QXQM-2, Changsha Tianchuang Powder Technology Co., Ltd., Changsha, China) at 200 rpm for 2 h. The collected slurry was separated using a rotary evaporator (R206B, Shanghai SENCO Technology Co., Ltd., Shanghai, China) and then dried in a vacuum drying chamber (DZF-6020, Shanghai Jinghong Laboratory Instrument Co., Ltd., Shanghai, China) for 24 h to remove residual ethanol. The as-received powder mixture was sieved through a 100-mesh sieve to minimise agglomeration. Subsequently, the powder was placed in a graphite die with an internal diameter of 50 mm and sintered in a spark plasma sintering furnace (D60, FCT Systeme GmbH, Rauenstein, Germany). As shown in Figure 3, four different sintering processes were designed: first, the temperature was increased from room temperature to 400 °C in 5 min and further to 1500 °C, 1550 °C, and 1600 °C at a speed of 100 °C/min, each held for 10 min. In another experiment, after the sintering temperature rose to 1600 °C, it dropped to 1550 °C within 10 min. Sintering was performed in an Ar atmosphere, and the axial pressure was maintained at 50 MPa. The samples prepared at the sintering temperatures of 1500 °C, 1550 °C, 1600 °C, and 1600→1550 °C are denoted as S1, S2, S3, and S4, respectively.

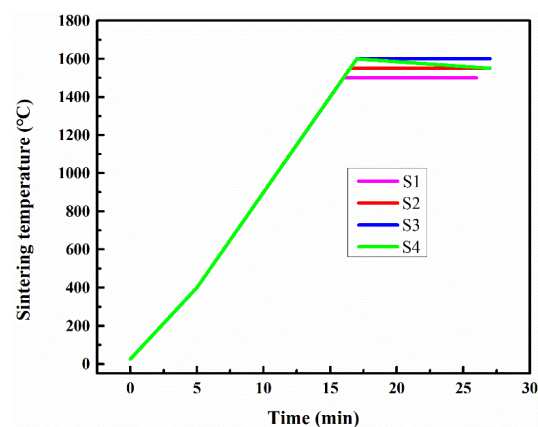


Figure 3. Variation in sintering temperature with time.

After sintering, the surfaces of the samples were levelled using a precision grinder (ACC-63DX, Okamoto Machinery Co., Ltd., Tokyo, Japan) and then cut into bars. Density was measured using the Archimedes method, and mechanical properties were tested using a ceramic testing system (CMT6503, Jinan Meitesi Testing Technology Co., Ltd., Jinan, China). The bending strength was measured via the three-point bending test on bars

sized 3 mm × 4 mm × 36 mm with a span of 30 mm and a loading rate of 0.5 mm/min. The fracture toughness was evaluated via the single-edge notched beam test on the 2.5 mm × 5 mm × 25 mm bars with a span of 20 mm and a loading rate of 0.05 mm/min. The final average values were determined using five bars. The phase components and microstructures were investigated using X-ray diffraction (XRD; PANalytical Empyrean, Einhorn, the Netherlands), scanning electron microscopy (SEM; Hitachi 3400, Tokyo, Japan), and field-emission scanning electron microscopy (FESEM; Hitachi/Regulus 8230, Tokyo, Japan) combined with energy-dispersive spectroscopy (EDS; Oxford/UltimMax 170, Oxford, UK). The Gibbs free energy of the reaction was evaluated using the chemical thermodynamics simulation software HSC Chemistry 6 (H: enthalpy, S: entropy, and C: heat capacity).

3. Results and Discussion

As shown in Figure 4, the size of large particles in the powder mixture after ball milling was around 20 µm, while Ti particles with a size close to 50 µm had disappeared. After ball milling, the diamond particles were preserved well because of their great hardness, and the Ti particles were effectively refined, which was considered to be beneficial to the process of reaction sintering.

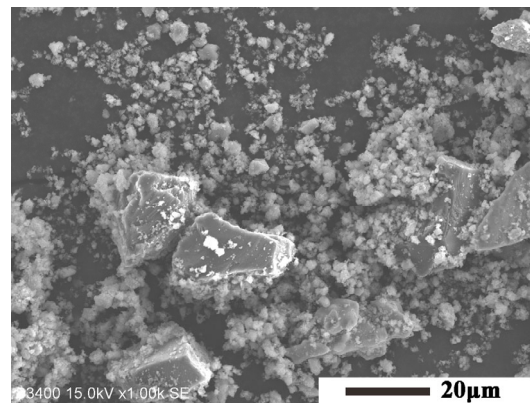


Figure 4. SEM image of diamond-Ti-Si powder mixture milled at 200 rpm for 2 h.

Figure 5 shows the XRD patterns of S1, S2, S3, and S4. Ti and Si disappeared from the spectra. The diamond peak intensity decreased gradually with increasing sintering temperatures, indicating increased diamond graphitisation. Simultaneously, the amounts of the main reaction products, SiC and TiC, increased. This is because, as the sintering temperature increased, both the carbon source (graphite) and the reaction-driving force increased simultaneously. As shown in Figure 5A, the intermediate product, TiB₂, existed only at sintering temperatures below 1500 °C. At 1550 °C, the XRD peak of TiSi₂ enhanced, and a new product, Ti₃SiC₂, appeared. Increasing the sintering temperature further enhanced the crystallinity and the diffraction peak intensity of TiSi₂. Because diamond graphitisation was increased at higher temperatures, C reacted with TiSi₂ to form Ti₃SiC₂. When the temperature rose to 1600 °C, the content and crystallinity of Ti₃SiC₂ were further increased. At this point, the diffraction peak of TiSi₂ disappeared, and in the presence of sufficient graphite, all the TiSi₂ was transformed into Ti₃SiC₂ according to Equation (1).



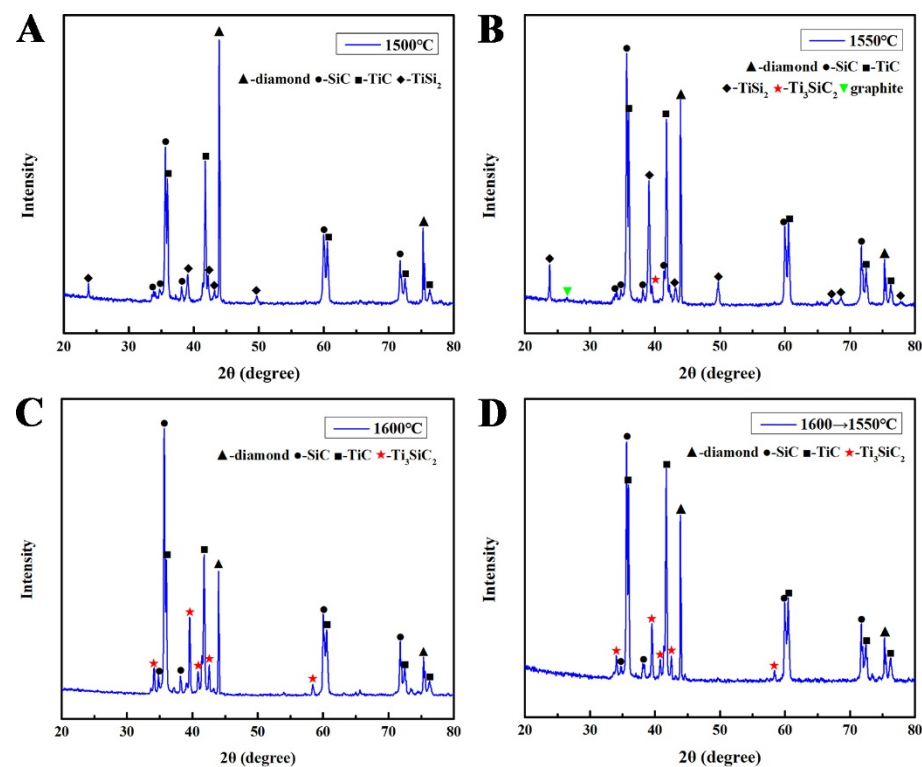


Figure 5. XRD patterns of diamond–ceramic composites sintered at different temperatures, (A) 1500 °C, (B) 1550 °C, (C) 1600 °C and (D) 1600→1550 °C.

Equation (1) also explains the synchronous increase in the XRD peak intensity of SiC in Figure 5C. As shown in Figure 5D, the temperature during the sintering of S4 dropped from 1600 °C to 1550 °C at a constant rate, and the average temperature of the whole process was <1600 °C. Consequently, more TiC was retained, resulting in a higher diffraction peak intensity for TiC than that for SiC in Figure 5C. Notably, only a weak graphite characteristic peak was observed in Figure 5B. Although diamond graphitises more easily at higher sintering temperatures, reaction (1) is easier to carry out, thus consuming more graphite. When the sintering temperature was 1600 °C, the composite was composed of diamond, SiC, TiC and Ti_3SiC_2 , and the semi-quantitative ratio analysis showed the phase composition was 21.4 wt%Diamond–39.8 wt%SiC–24.1 wt%TiC–14.7 wt% Ti_3SiC_2 .

Figure 6A shows a backscattered electron scanning image of the fracture surface. The black regions with the highest carbon concentration correspond to diamond grains. The grey-black regions with the highest Si concentration and a moderate C concentration correspond to SiC grains. The grey-white regions representing the highest Ti concentration with some Si or C elements correspond to TiC or TiSi_2 grains.

As shown in Table 1, the volume densities of the diamond–ceramic composites gradually decreased with increasing sintering temperatures. The phase differences between S1, S2, S3, and S4 prepared at four different sintering temperatures were mainly caused by reaction (1). The parameters of the reactants and products of this reaction are listed in Table 2. Evidently, the volume density of the reactants was 4.60 g/cm³, which is higher than that of the products (4.21 g/cm³).

Table 1. Volume density of diamond–ceramic composites sintered at different temperatures.

Samples	S1 (1500 °C)	S2 (1550 °C)	S3 (1600 °C)	S4 (1600→1550 °C)
Volume density (g/cm ³)	3.647	3.604	3.555	3.596

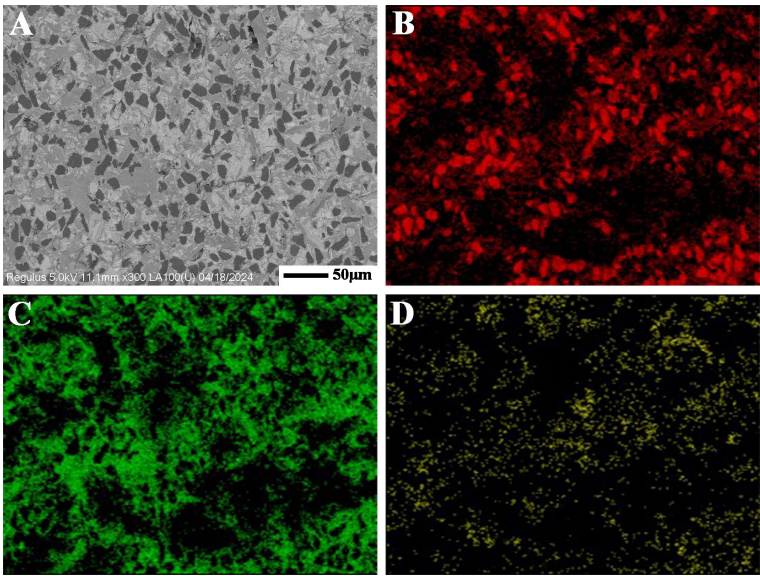


Figure 6. Element distribution of the diamond–ceramic composite sintered at 1500 °C: (A) backscattered electron image, (B) C, (C) Si, (D) Ti.

Table 2. Properties of the reactants and products in reaction (1).

Reactants				Products	
Matter	2TiC	TiSi ₂	C	Ti ₃ SiC ₂	SiC
Relative atomic mass	119.76	104.05	12.01	195.72	41
Density/(g/cm ³)	4.93	4.39	3.52	4.53	3.2
	4.60			4.21	

Figure 7 shows the fracture surfaces of the diamond–ceramic composites. The samples prepared at different sintering temperatures exhibited a high degree of densification. However, some holes with larger dimensions were observed, as indicated by the yellow arrows. Compared to the results in Figure 2A, these holes were only slightly smaller than the raw diamond particles. This implies that these holes were caused by the elimination of the diamond particles. Moreover, Figure 7 shows that the number of holes on the fracture surface increased with increasing sintering temperature. At high temperatures, diamond transformed into graphite, which possessed a weak interlayer binding force. Therefore, after the outer layer of the diamond graphitised, the diamond particles were easily removed when the material fractured. The graphitisation rate of diamond increased with increasing sintering temperature, and because the graphite could not react with Ti or Si over time, the pull-out phenomenon of diamond particles increased. Although no graphite phase was detected in the XRD patterns, it can be inferred that a small amount of graphite was present in these samples. This is also why the volume density of the sample decreased with increasing sintering temperature.

As shown in Figure 8A, the fracture toughness of the diamond–ceramic composites decreased with increasing sintering temperature. The fracture surfaces in Figure 7 reveal that the fracture mode of the diamond–ceramic composite was a combination of transgranular and intergranular fractures. Intergranular fractures contributed to the toughening of crack deflection [22]. Crack deflection mainly occurred around the diamond phase because the thermal expansion coefficients of the diamond and ceramic phases differed significantly, and an interface with a weak bonding force was formed after diamond graphitisation. The prolonged cracks caused by crack deflection consumed more fracture energy, resulting in increased fracture toughness [23]. The degree of crack deflection depends on the size

of the diamond particles, and the energy consumed per unit length of the crack depends on the interface bonding strength. With increasing sintering temperature, the degree of graphitisation of the diamond increased, thus decreasing the diamond size and weakening the interface bonding. Consequently, the fracture toughness of the diamond–ceramic composite was reduced.

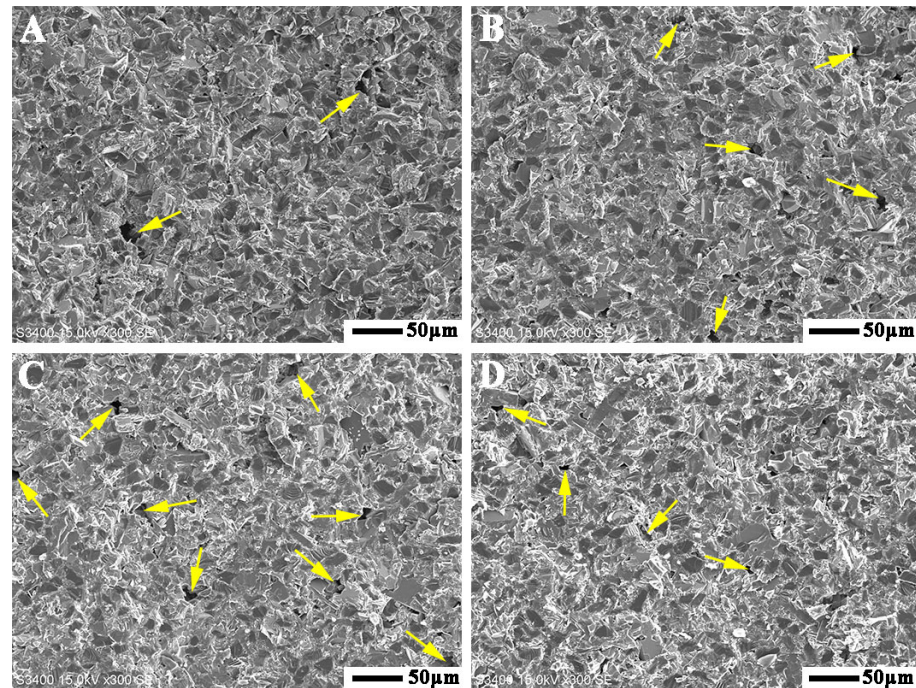


Figure 7. SEM images of diamond–ceramic composites sintered at different temperatures, (A) 1500 °C, (B) 1550 °C, (C) 1600 °C and (D) 1600→1550 °C.

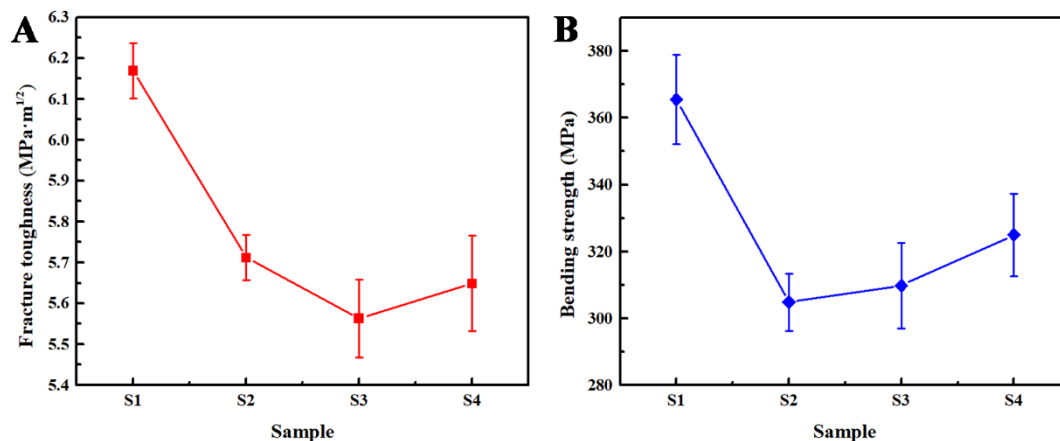


Figure 8. Fracture toughness (A) and bending strength (B) of diamond–ceramic composites sintered at different temperatures.

As shown in Figure 8B, the bending strength was the lowest when the sintering temperature was 1550 °C. At this temperature, although the graphitisation of the diamond was low, its size was only slightly reduced; however, graphite was not consumed in time, resulting in an extremely weakened diamond interface. This resulted in larger defects that cause crack initiation in S2, resulting in easy failure under load [24]. When the sintering temperature rose to 1600 °C, the size of the diamond was further reduced, and graphite was consumed by reaction (1), resulting in a slightly higher bending strength of S3 than

that of S2. In summary, when the sintering temperature was 1500 °C, the bending strength and fracture toughness reached 366 MPa and 6.17 MPa·m^{1/2}, respectively. Therefore, the optimal sintering temperature is 1500 °C. As shown in Table 3, the mechanical properties of this work are superior to those of the same types of materials.

Table 3. Bending strength and fracture toughness of diamond–ceramic composites.

Sample	Bending Strength (MPa)	Fracture Toughness (MPa·m ^{1/2})	Ref.
Diamond–SiC–TiC	366	6.17	This work
Diamond–SiC	248	4.65	[25]
SiC–Diamond	400	4.5	[26]
Diamond–SiC	287	5.0	[27]
Diamond–SiC	237	—	[28]
Diamond–SiC	378	4.0	[29]

Compared with XRD, Raman spectroscopy is more sensitive in detecting graphite. Therefore, Raman spectroscopy was performed to characterise the reaction product accumulation area around the diamond. As shown in Figure 9, the characteristic peaks at 796 cm^{−1} and 970 cm^{−1} correspond to SiC, and the characteristic peak of graphite was observed at 1524 cm^{−1} [30]. Although the average temperature of S4 was higher than that of S2, the higher initial temperature activated reaction (1), resulting in higher graphite consumption and a weaker characteristic peak strength of graphite in S4 than that in S2. Consequently, the diamonds in S4 had smaller sizes and stronger interfacial bonds. This unique variable-temperature sintering results in a higher bending strength of S4 than that of S2 and S3.

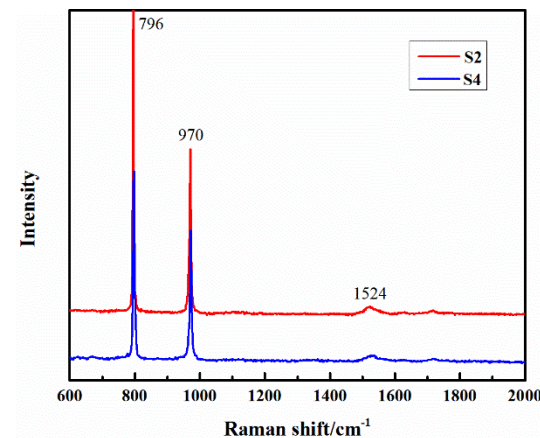


Figure 9. Raman spectra of diamond–ceramic composites sintered at different temperatures.

Figure 10A,B show the line-scan images of the diamond–ceramic composite. The grey-white, grey-black, and black regions correspond to Ti₃SiC₂, SiC, and diamond, respectively. Figure 10C shows an enlarged image of Line 1 (yellow line), and the structure of the above regions can be determined after analysis in combination with Figure 10D. As shown in Section I of Figure 10C, Ti, Si, and C were present simultaneously with their stable contents, confirming that this region was Ti₃SiC₂. In Section II, Ti disappeared, the Si content increased, and the Si and C contents were relatively stable, indicating the region as SiC. Section III contained only Si and C elements; however, their contents were unstable, indicating that a part of this region was graphite and the other part was a solid solution formed after Si elements were diffused into the diamond. The remaining area contained only C with a stable content, indicating a stable structure of diamond. Complex structures around diamonds were formed by a combination of diffusion, phase transitions, and chemical reactions.

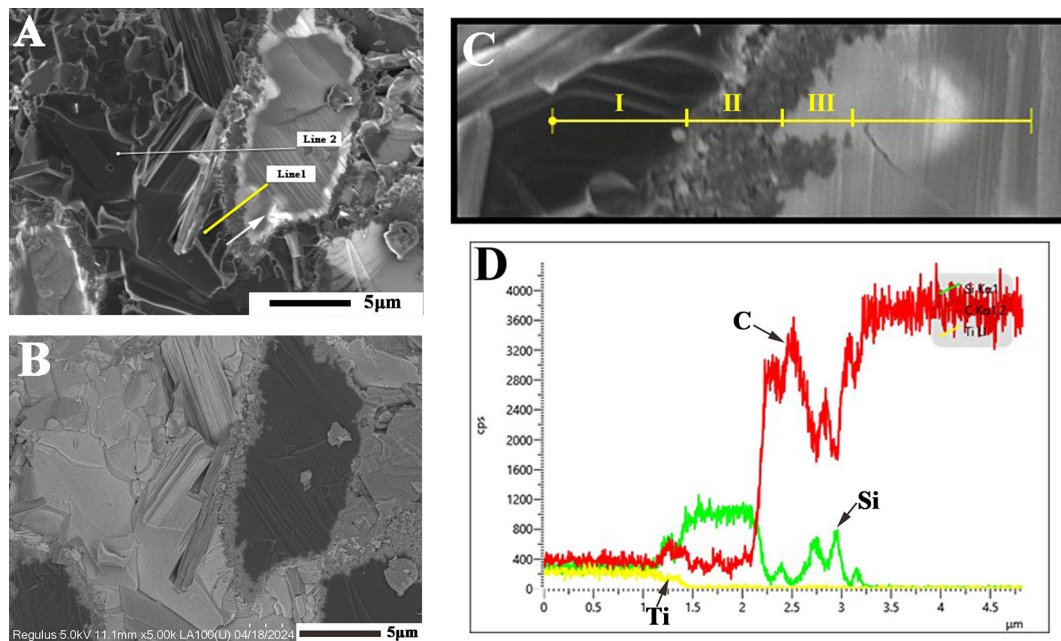


Figure 10. Line-scan element distribution images of the diamond–ceramic composite sintered at 1500 °C, (A) SEM image, (B) BSE image, (C) enlarged view of the line sweep area and (D) element content.

4. Conclusions

Diamond–SiC composites are generally prepared by Si infiltration or HTHP (high temperature high pressure). The above methods easily cause Si residue and have strict requirements for the equipment. In this study, the silicon residue in the composite was eliminated by introducing Ti, which reacted more easily with graphite. In addition, the conductivity of the composite was improved, which was conducive to improving the machinability. The following conclusions were drawn:

- (1) Through the absorption of graphite by Ti and Si, the liquid phase provided by Si, and spark plasma sintering, diamond–ceramic composites were successfully prepared under conventional conditions.
- (2) Characteristic of variable-temperature sintering, the chemical reaction was activated at a higher temperature, and then the sintering temperature was reduced to prevent excessive graphitisation. This method is particularly suitable for preparing diamond–ceramic composites and has certain research value.

Author Contributions: Conceptualisation, L.H.; methodology, L.H.; software, A.W.; validation, A.W.; formal analysis, Y.S.; investigation, Y.S.; resources, C.L.; data curation, C.L.; writing—original draft, Y.S.; writing—review and editing, Q.H. and W.W.; supervision, Q.H.; project administration, W.W.; funding acquisition, Q.H. All authors have read and agreed to the published version of the manuscript.

Funding: This work is supported by the National Natural Science Foundation of China (52102074), the National Key Research and Development Plan of China (2021YFB3701400), the Fundamental Research Funds for the Central Universities (WUT:2024IVA002), the Natural Science Foundation of Hubei Province (2022CFD118), and the State Key Laboratory of Advanced Technology for Materials Synthesis and Processing, Wuhan University of Technology (2023-KF-14).

Institutional Review Board Statement: Not applicable.

Informed Consent Statement: Not applicable.

Data Availability Statement: The original contributions presented in this study are included in the article; further inquiries can be directed to the corresponding author.

Conflicts of Interest: The authors declare no conflict of interest. The funders had no role in the design of the study; in the collection, analyses, or interpretation of data; in the writing of the manuscript, or in the decision to publish the results.

References

- Shul'zhenko, A.A.; Sokolov, A.N.; Gargin, V.G. New Diamond-Based Superhard Materials. Production and Properties. Review. *J. Superhard Mater.* **2018**, *40*, 304–314. [\[CrossRef\]](#)
- Zhang, J.B.; Wang, J.P.; Zhang, G.Q.; Huo, Z.X.; Huang, Z.J.; Wu, L.J. A review of diamond synthesis, modification technology, and cutting tool application in ultra-precision machining. *Mater. Des.* **2024**, *237*, 112577. [\[CrossRef\]](#)
- Chen, F.; Yan, Z.Q.; Liu, Z.P.; Long, Y.; Fu, N.K.; Zhang, F.L.; Liu, B.; Liu, Y. Preparation and properties of Al₂O₃-reinforced Cu-Ni-Sn metallic matrix for applications in diamond-cutting tools. *Diam. Relat. Mater.* **2020**, *109*, 108025. [\[CrossRef\]](#)
- Xiang, J.F.; Pang, S.Q.; Xie, L.J.; Gao, F.N.; Hu, X.; Yi, J.; Hu, F. Mechanism-Based FE Simulation of Tool Wear in Diamond Drilling of SiC_p/Al Composites. *Materials* **2018**, *11*, 252. [\[CrossRef\]](#) [\[PubMed\]](#)
- Zhou, H.Y.; Jia, Q.J.; Sun, J.; Li, Y.Q.; He, Y.S.; Bi, W.S.; Zheng, W.Y. Improved Bending Strength and Thermal Conductivity of Diamond/Al Composites with Ti Coating Fabricated by Liquid-solid Separation Method. *Materials* **2024**, *17*, 1485. [\[CrossRef\]](#) [\[PubMed\]](#)
- Zhang, Y.J.; Bai, G.Z.; Zhu, X.Y.; Dai, J.J.; Wang, X.T.; Wang, J.G.; Kim, M.J.; Zhang, H.L. Manipulating in-situ discrete carbide interlayer to achieve high thermal conductivity in Cu-B/diamond composite. *Mater. Today Commun.* **2023**, *34*, 105357. [\[CrossRef\]](#)
- Li, M.; Sun, Y.H.; Meng, Q.N.; Wu, H.D.; Gao, K.; Liu, B.C. Fabrication of Fe-Based Diamond Composites by Pressureless Infiltration. *Materials* **2016**, *9*, 1006. [\[CrossRef\]](#)
- Aldwell, B.; Yin, S.; McDonnell, K.A.; Trimble, D.; Hussain, T.; Lupoi, R. A novel method for metal-diamond composite coating deposition with cold spray and formation mechanism. *Scripta. Mater.* **2016**, *115*, 10–13. [\[CrossRef\]](#)
- Wei, C.L.; Wang, X.X.; Tong, P.; Wang, P.; Wen, J. Effect of different titanium addition methods on the properties of diamond/Cu composites. *J. Mater. Res. Technol.* **2024**, *31*, 2014–2022. [\[CrossRef\]](#)
- Ekimov, E.A.; Borovikov, N.F.; Ivanov, A.S.; Pal, A.F.; Rusinkevich, A.A.; Serov, A.O.; Starostin, A.N.; Fortov, V.E.; Gromnitskaya, E.L. Application of the dusty plasma method for preparation of diamond ceramics. *Diam. Relat. Mater.* **2014**, *41*, 1–5. [\[CrossRef\]](#)
- Kailer, A.; Matthey, B.; Kunze, S.; Herrmann, M.; Tschirpke, C. SiC-bonded diamond ceramics for extreme conditions in subsea applications. *Int. J. Appl. Ceram. Technol.* **2024**, *21*, 2690–2701. [\[CrossRef\]](#)
- Qian, J. High-pressure, high-temperature sintering of diamond-SiC composites by ball-milled diamond-Si mixtures. *J. Mater. Res.* **2002**, *17*, 2153–2160. [\[CrossRef\]](#)
- Herrmann, M.; Matthey, B.; Höhn, S.; Kinski, I.; Rafaja, D. Diamond-ceramics composites—New materials for a wide range of challenging applications. *J. Eur. Ceram. Soc.* **2012**, *32*, 1915–1923. [\[CrossRef\]](#)
- Zhang, J.W.; Zhan, G.D.; He, D.W.; Li, D.; Li, Q.; Du, C.C.; Dai, Q.S.; Liu, F.M.; Yan, X.Z. Transparent diamond ceramics from diamond powder. *J. Eur. Ceram. Soc.* **2023**, *43*, 853–861. [\[CrossRef\]](#)
- Jaworska, K.; Gibas, T.; Wyczesany, A.; Królicka, B.; Rajchel, B. Study on interactions in diamond-ceramic material systems. *J. Mater. Process. Technol.* **2003**, *133*, 118–121. [\[CrossRef\]](#)
- Lai, S.L.; Zang, J.H.; Shen, W.X.; Huang, G.F.; Fang, C.; Zhang, Y.W.; Chen, L.C.; Wang, Q.Q.; Wan, B.; Jia, X.P.; et al. High hardness and high fracture toughness B₄C-diamond ceramics obtained by high-pressure sintering. *J. Eur. Ceram. Soc.* **2023**, *43*, 3090–3095. [\[CrossRef\]](#)
- Beffort, O.; Vaucher, S.; Khalid, F.A. On the thermal and chemical stability of diamond during processing of Al/diamond composites by liquid metal infiltration. *Diam. Relat. Mater.* **2004**, *13*, 1834–1843. [\[CrossRef\]](#)
- Zhu, C.X.; Lang, J.; Ma, N.G. Preparation of Si-diamond-SiC composites by in-situ reactive sintering and their thermal properties. *Ceram. Int.* **2012**, *38*, 6131–6136. [\[CrossRef\]](#)
- Liu, G.; Wang, A.Y.; Tang, R.; Bai, W.H.; Song, Y.W.; Ji, W.; Wang, W.M. Fabrication and modeling of ultra-hard and high-strength B₄C-based laminated ceramics by brazing joining. *Ceram. Int.* **2022**, *48*, 27982–27987. [\[CrossRef\]](#)
- Zhou, L.; Li, Y.Y.; Kou, Z.L.; Zheng, L.P.; Li, Q.; Ma, G.L.; Zhang, Y.J.; He, D.W. Heterogeneous diamond-TiC composites with high fracture toughness and electrical conductivity. *J. Eur. Ceram. Soc.* **2024**, *44*, 4887–4894. [\[CrossRef\]](#)
- Zhou, X.L.; Wang, Y.H.; Li, T.H.; Li, X.H.; Cheng, X.Z.; Dong, L.; Yuan, Y.G.; Zang, J.B.; Lu, J.; Yu, Y.Q.; et al. Fabrication of diamond-SiC-TiC composite by a spark plasma sintering-reactive synthesis method. *J. Eur. Ceram. Soc.* **2015**, *35*, 69–76. [\[CrossRef\]](#)
- Yoshida, K.; Nishiyama, N.; Shinoda, Y.; Akarsu, T.; Wakai, F. Evaluation of effects of crack deflection and grain bridging on toughening of nanocrystalline SiO₂ stishovite. *J. Eur. Ceram. Soc.* **2017**, *37*, 5113–5117. [\[CrossRef\]](#)
- Wang, A.Y.; He, Q.L.; Guo, W.C.; Liu, C.; Tian, T.; Hu, L.X.; Liu, L.S.; Wang, W.M.; Fu, Z.Y. Microstructure and properties of hot pressed TiB₂ and SiC reinforced B₄C-based composites. *Mater. Today Commun.* **2021**, *26*, 102082. [\[CrossRef\]](#)
- Tian, S.; Guo, W.C.; He, Q.L.; Wang, A.Y.; Tian, T.; Liu, C.; Hu, L.X.; Zhang, Z.X.; Wang, H.; Wang, W.M.; et al. Synthesis of TiN-TiB₂-hBN composites powders with a core-shell structure and preparation of bulk samples. *Mater. Today Commun.* **2021**, *29*, 102783. [\[CrossRef\]](#)
- Chen, C.; Liu, Y.S.; Wang, C.H.; Nan, B.Y.; Zhao, Z.F.; Cheng, L.F.; Zhang, L.T. Microstructure and Properties of Diamond/SiC Composites Via Hot Molding Forming and CVI Densifying. *Adv. Eng. Mater.* **2019**, *21*, 1800640. [\[CrossRef\]](#)

26. Matthey, B.; Kunze, S. SiC-bonded diamond materials produced by pressureless silicon infiltration. *J. Mater. Res.* **2017**, *32*, 3362–3371. [[CrossRef](#)]
27. Zhao, Z.F.; Liu, Y.S.; Feng, W.; Zhang, Q.; Cheng, L.F.; Zhang, L.T. Improvement on the thermal conductivity of Diamond/CVI-SiC composites using diamond particles. *Diam. Relat. Mater.* **2017**, *74*, 1–8. [[CrossRef](#)]
28. Hong, T.X.; Chen, Y.H.; Liu, R.B.; Hai, W.X.; Zhang, X.L.; Liu, M.L.; Yan, S. Effect of infiltration temperature on graphitization and properties of diamond/SiC composites with SiC matrix. *Int. J. Appl. Ceram. Technol.* **2024**, *21*, 1829–1838. [[CrossRef](#)]
29. Liu, Y.S.; Hu, C.H.; Men, J.; Feng, W.; Cheng, L.F.; Zhang, L.T. Effect of diamond content on microstructure and properties of diamond/SiC composites prepared by tape-casting and CVI process. *J. Eur. Ceram. Soc.* **2015**, *35*, 2233–2242. [[CrossRef](#)]
30. Ferrari, A.C. Raman spectroscopy of graphene and graphite: Disorder, electron–phonon coupling, doping and nonadiabatic effects. *Solid State Commun.* **2007**, *143*, 47–57. [[CrossRef](#)]

Disclaimer/Publisher’s Note: The statements, opinions and data contained in all publications are solely those of the individual author(s) and contributor(s) and not of MDPI and/or the editor(s). MDPI and/or the editor(s) disclaim responsibility for any injury to people or property resulting from any ideas, methods, instructions or products referred to in the content.